Journal of Nuclear Materials 397 (2010) 31–35

Contents lists available at ScienceDirect

Journal of Nuclear Materials

journal homepage: www.elsevier.com/locate/jnucmat

Pulsed laser nitriding of uranium

Yongbin Zhang [a,*], Daqiao Meng [a], Qinying Xu [a], Youshou Zhang [b]

[a] State Key Laboratory for Surface Physics and Chemistry, P.O. Box 718-35, Mianyang, Sichuan 621907, China
[b] China Academy of Engineering Physics, P.O. Box 919, Mianyang, Sichuan 621900, China

ARTICLE INFO

Article history:
Received 19 June 2009
Accepted 4 December 2009

ABSTRACT

Pulsed laser nitriding offers several advantages such as high nitrogen concentration, low matrix temperature, fast treatment, simple vacuum chamber and precise position control compare to ion implantation, which is favorable for radioactive material passivation. In this work, uranium metal was nitrided using an excimer laser for the first time. The nitrided layers are characterized by X-ray diffraction, X-ray photoelectron spectroscopy and scanning electron microscopy. The nitride layer is composed mainly of UN and U_2N_3 and depends on nitriding process. The amount of nitride increases with energy density and pressure. The irradiated area has a wavy structure which increases the roughness, while scratches and asperities caused by sand paper polishing were eliminated. Scan speed has a profound influence on the nitride layer, at low speed U_2N_3 is more likely to form and the nitride layer tends to crack. XPS analysis shows that nitrogen has diffused into interior, while oxygen is only present on the surface. Ambient and humid–hot corrosion tests show the nitrided sample has good anticorrosion property.

1. Introduction

Uranium metal readily corrodes under the ambient environment. Many technologies including physical vapor deposition and ion implantation were developed to improve its corrosion resistance [1–4]. Physical vapor deposition has the drawback of discontinuous interfaces between the coatings and substrate, which makes the coatings fall off. Ion implantation produces thin modified surface layers which avoid the formation of discontinuous interfaces typical to coatings, but the temperature rise caused by ion implantation is very high and effective cooling is needed. Moreover these techniques are performed in vacuum chamber consisted of target, ion source and specimen moving system which are easily contaminated by radioactive materials. The contaminated equipment is difficult to maintaining.

Pulsed laser nitriding has been studied on metals and the metal-nitride layer produced by a high-power pulsed laser greatly improves the surface hardness and the corrosion resistance [5–7]. Compared to the ion implantation method, pulsed laser nitriding offers several advantages such as low matrix temperature, fast treatment and precise position control [8]. Moreover the vacuum chamber can be simple in form without cooling system, specimen moving system (using laser scan externally), target and ion source, which is favorable for treating radioactive materials. However, up to now, no research has been reported on nitriding of actinide metal. In this work, uranium metal is nitrided using an excimer and samples were characterized by X-ray diffraction, X-ray photoelectron spectroscopy and scanning electron microscopy. The uranium nitride layer was formed and corrosion tests show that the nitrided sample has good anticorrosion property.

2. Experimental

The uranium samples (20 mm diameter, 2 mm thickness) were polished down to 500 mesh by sand paper then cleaned with acetone followed by ethanol. The irradiation chamber was evacuated to 1 Pa before it was filled with 99.99% pure nitrogen gas. The samples were irradiated with a Lambda Physik excimer laser (wavelength $\lambda = 248$ nm, pulsed width 25 ns). The laser beam was focused on the sample by a convex lens with spot size of 1×2 mm^2. Energy density was set by adjusting the output energy of the laser, which was monitored by a thermoelectric energy detector. In order to treat extended areas, the vacuum chamber was placed on a two dimensional motorized linear stage. The laser scan along *X* direction with speed changed from 0.1 to 1.28 mm/s. After scanning a line in *X* direction, the vacuum chamber moved 1 mm along *Y* direction. The two steps repeated until full area of the uranium sample was irradiated. A series of treated samples were characterized with several methods. For clarity, typical results for selected samples are presented in the paper. The surface morphology microstructure of the nitrided samples was examined by scanning electron microscopy (SEM). The crystallographic properties were identified by X-ray diffraction (XRD) analysis

* Corresponding author.
E-mail address: zybzyb9062@gmail.com (Y. Zhang).

0022-3115/$ - see front matter © 2009 Elsevier B.V. All rights reserved.
doi:10.1016/j.jnucmat.2009.12.002

performed using CuKα radiation with a graphite monochromater. The chemical composition and depth distribution of the treated uranium samples were analyzed by X-ray photoelectron spectroscopy (XPS). The argon ion gun was operated at 3.0 kV, the uranium sputtering rate was estimated to be 3 nm/min. After nitriding, samples were subjected to a series of corrosion tests, including ambient corrosion, hot humid corrosion test (temperature 90 °C, humidity 95%). For the ambient corrosion test, the sample was placed for 1 year in laboratory ambient and XRD analysis was performed every two months.

3. Results and discussion

3.1. Phase analysis

Phases present in samples irradiated under different energy density, scan speed and nitrogen pressure were characterized by X-ray diffraction analysis. For clarity only selected samples are shown in Fig. 1. The standard α-uranium has four strong peaks at 34.94°, 35.56°, 36.31°, 39.57° (PDF#65-5713), associated with the planes of (110), (021), (002) and (111) respectively. From the XRD analysis it can be seen that the peak of (002) plane for the as-received untreated uranium is far more stronger than three others. It can be argued that the untreated uranium samples had a highly preferred orientation, which probably caused by mechanical abrasion or machining. After nitriding, the peak of (110) plane for uranium becomes strongest, the peaks of (021), (002) plane become very small. Laser irradiation of uranium under argon atmosphere was also performed. The XRD spectra is similar to that of metallic uranium peak for nitrided samples, it can be seen no other phase of metallic uranium has been formed. After nitriding uranium mononitride can be identified. The lattice constant of UN was determined to be 0.4853 nm, while the standard lattice constant is around 0.4890 nm (PDF#89-5216). The peak near 28.70° was attributed to U_2N_3. Though the UO_2 has peak near 28.30°, the XPS depth profile shows that the UO_2 is very thin (~3 nm). Grazing incident diffraction was performed at 3° to obtain qualitative information on phase of the surface (Fig. 2). It can be seen that the relative area of the uranium peaks decreases about 70% within the penetration depth of uranium (250 nm) at 3° X-ray incidence. Therefore the phases present near the surface is mainly composed of the nitride. The peak of U_2N_3 moves to 28.90°. As the uranium has no peak near 28.70°, the influence of uranium can be excluded. The lattice constant of U_2N_3 beneath surface was determined to be 1.076 nm, while the lattice constant of uranium nitride at surface is around 1.0699 nm. The lattice increase can be attributed to nitrogen deficiency as it is often observed in uranium nitride [13]. For a small change of lattice constant with treatment parameter is also observed. For energy densities below 1.0×10^{-2} J/mm^2, no uranium nitride formed. The amount of nitride increases with energy density, pressure. Laser scan speed has profound influence on the nitride layer, at low speed U_2N_3 is more likely to form. The amount of nitride decrease with increased scan speed as the number of pulses radiating the sample is inversely proportional with scan speed. The nitrogen concentration and nitride phase change with processing parameters will be presented in more detail in the next paper.

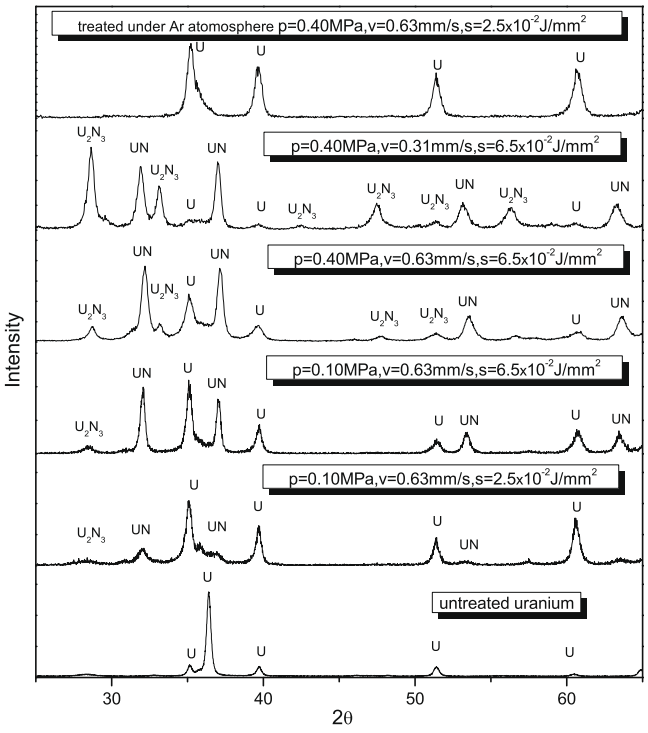

Fig. 1. Selected XRD spectra of nitrided uranium, conditions p: nitrogen pressure, v: scan speed of sample, s: energy density.

3.2. Morphology analysis

The contrast between irradiated and non-irradiated area was readily seen visually after nitriding, the irradiated area being darker but still has metallic luster. The roughness of the non-irradiated area was $R_a = 0.03$ μm and that of irradiated area was $R_a = 0.5$ μm. Low and high magnification planar view scanning electron microscopy (SEM) photomicrographs are presented in Fig. 3a–c, respectively, of laser nitrided and non-nitrided area. The morphology of the laser nitrided surface shows wavy structure which increases the roughness. The non-irradiated areas had many scratches and asperities, while at irradiated area, scratches, asperities were eliminated. The eliminating of asperities could be ascribed the flowing or flattening of softening and melting material under the effect of surface tension. At low scan speed, high nitrogen pressure and high energy density, the laser formed nitride layer tends to crack as shown in Fig. 3d. Among these factors laser scan speed has greatest effect on the cracking. At speeds >1.28 mm/s even energy density >8.5×10^{-2} J/mm^2 and nitrogen

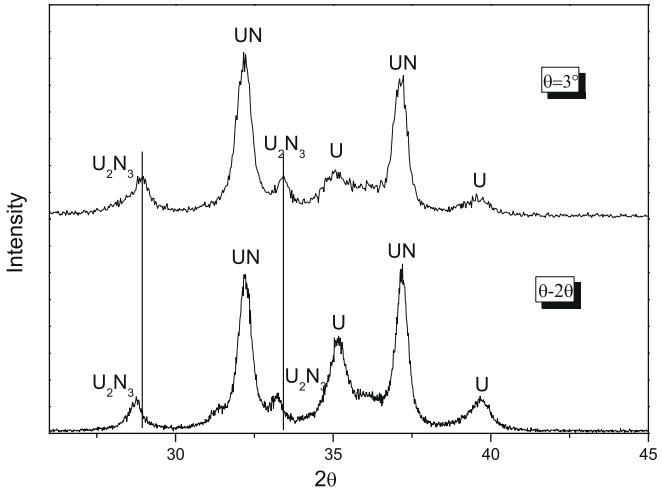

Fig. 2. Grazing incident XRD spectra of nitrided uranium sample prepared at scan speed of 0.63 mm/s, energy density of 6.5×10^{-2} J/mm^2 and nitrogen pressure of 0.4 MPa.

pressure >0.8 MPa, the nitride layer does not crack. However, at speed of 0.3 mm/s, energy density of 4.5×10^{-2} J/mm^2 and nitrogen pressure of 0.2 MPa the layer cracks. Experiment of multiple shots on the same area was also conducted, even shots more than 500 did not make surface crack. (The laser spot area is 1×2 mm^2, overlapping of laser scanning lines is 50%. At scan speed of 0.1 mm/s, a 1×2 mm^2 area received 20 laser spots.) So cracking has much to do with scanning process. The mechanism of cracking will study

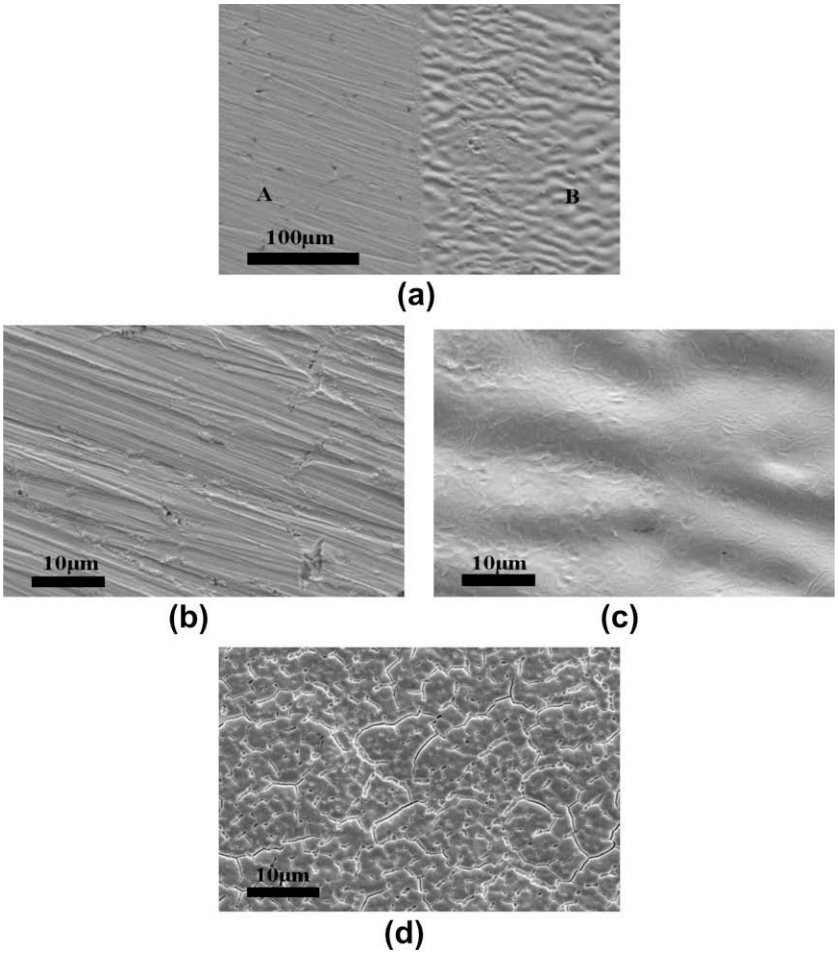

Fig. 3. A SEM micrograph of uranium sample: (a) low magnification showing non-irradiated Region A and irradiated Region B, (b) and (c) 2000× photomicrographs of the two regions, (d) crack of nitride layer prepared at scan speed of 0.31 mm/s, energy density of 4.5×10^{-2} J/mm^2 and nitrogen pressure of 0.4 MPa.

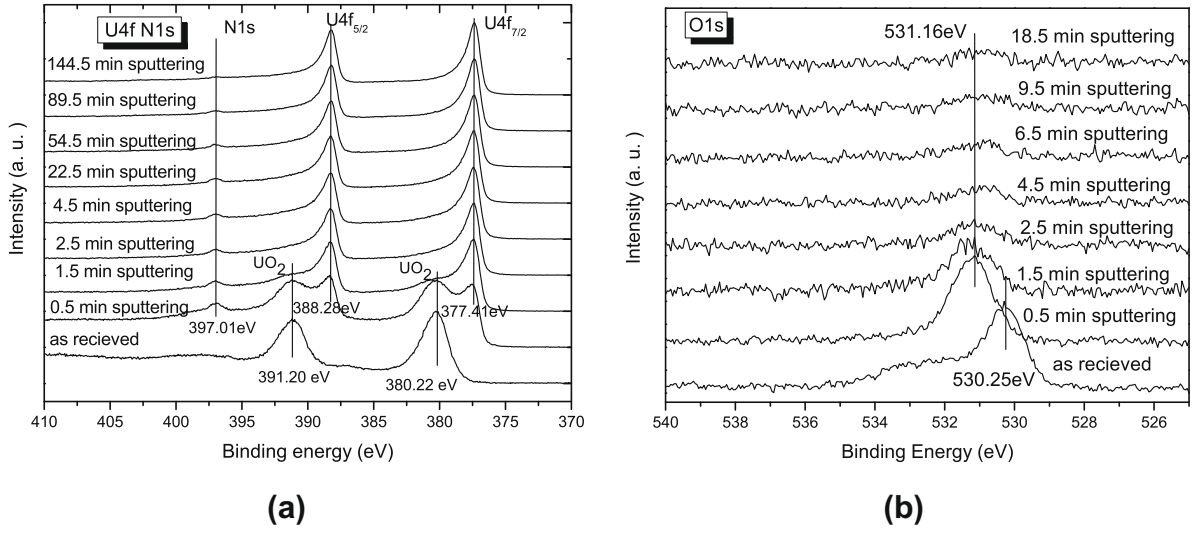

Fig. 4. *U4f*$_{7/2,5/2}$ N1s O1s core-level spectra versus sputtered depth for layer prepared at scan speed of 0.63 mm/s, energy density of 6.5×10^{-2} J/mm^2 and nitrogen pressure of 0.6 MPa; (a) *U4f*$_{7/2,5/2}$ N1s core spectra (b) O1s core spectra.

in future with help of multi-physical fields finite element simulation.

3.3. Corrosion tests

The corrosion testings were done on sample prepared at scan speed of 0.63 mm/s, energy density of 6.5×10^{-2} J/mm^2 and nitrogen pressure of 0.6 MPa. Fig. 4 presents the $U4f_{7/2,5/2}$ core-level spectra for the pulsed laser nitrided uranium, respectively, as a function of sputter etch time. The measured $U4f_{7/2,5/2}$ spin–orbit pair binding energies for the nitrided sample sputtered surfaces are 390.2 eV and 391.2 eV, respectively, in agreement with literature values for uranium in a U^{4+} valence state [9,10]. After 0.5 min sputtering, new peaks of binding energy 388.3 eV, 377.4 eV and 397.0 eV emerge, which are in agreement with values for $U4f_{7/2,5/2}$, N1s O1s core-level for UN [11]. As sputtering depth increases the peaks for UO_2 rapidly disappear. The O1s spectra has the similar trend as $U4f_{7/2,5/2}$. The N1s core spectra is overlapped with $U4f_{5/2}$ peak tail, the peak curve of $U4f_{5/2}$ and N1s were fitted and peak area was calculated. The associated elemental ratios versus depth are presented in Fig. 5 calculated using instru-

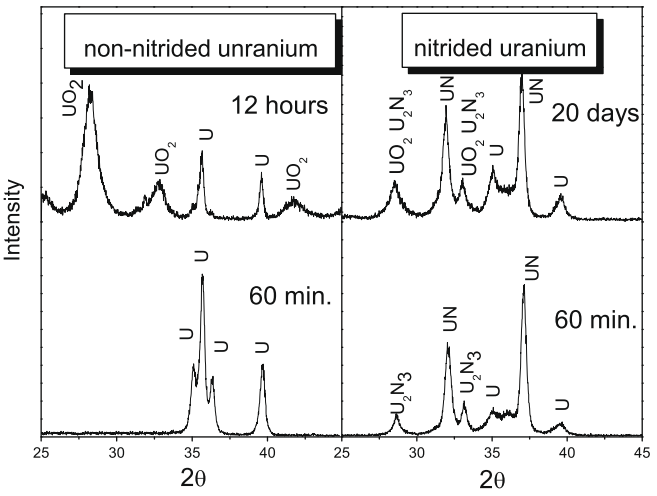

Fig. 7. X-ray diffraction (XRD) spectra of the laser nitrided and of the non-nitrided uranium samples that was subjected to hot–humid corrosion test.

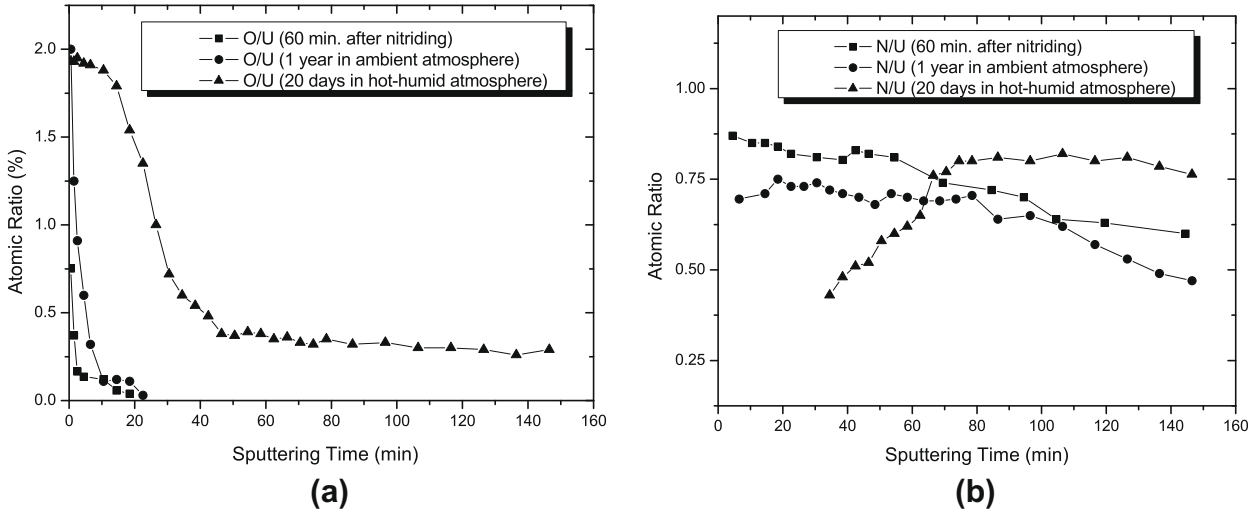

Fig. 5. Changes in O/U and N/U ratios with depth of uranium sample 60 min after nitriding, 1 year in ambient atmosphere and 20 days hot–humid corrosion, 0.63 mm/s, energy density 6.5×10^{-2} J/mm^2 and nitrogen pressure 0.6 MPa, (a) O/U ratio (b) N/U ratio.

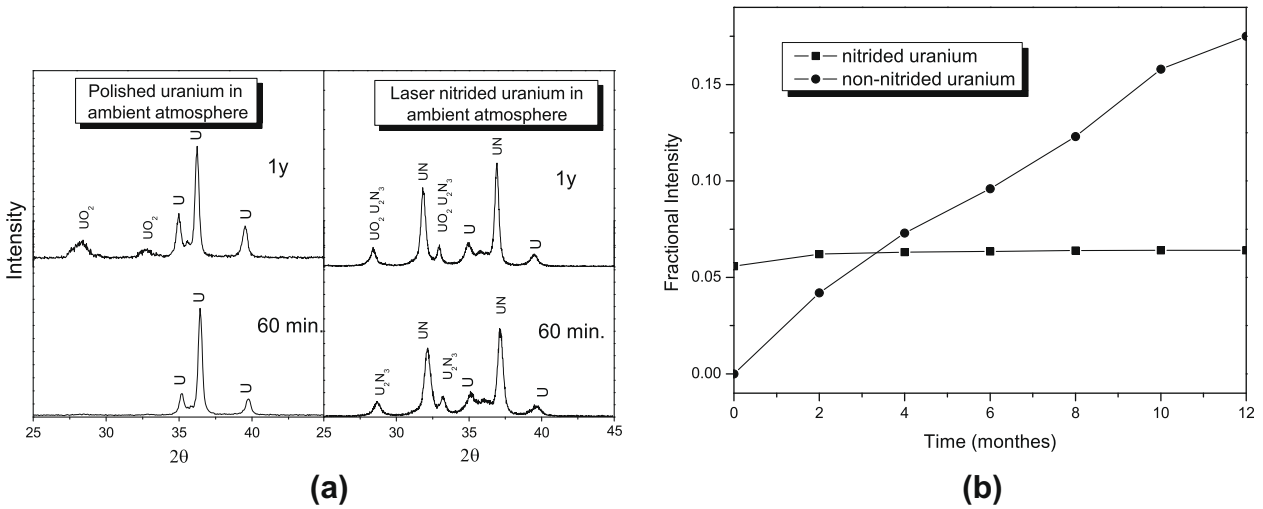

Fig. 6. X-ray diffraction (XRD) spectra of the laser nitrided and of the non-nitrided uranium samples that were kept for 1 year under ambient atmosphere. (a) XRD spectras, (b) fractional intensity of peak at $\theta = 28.5°$.

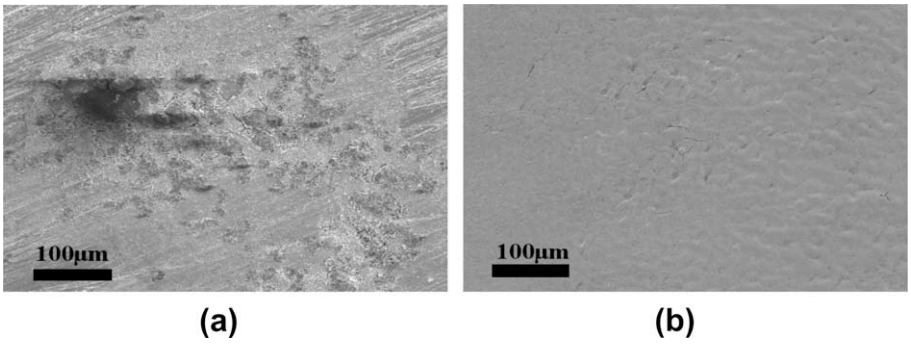

Fig. 8. SEM micrograph of uranium sample under hot–humid corrosion test: (a) non-nitrided uranium sample in hot–humid environment 12 h, (b) laser nitrided uranium sample under hot–humid environment for 20 days.

ment specific relative sensitivity factors with the measured core-level peak areas. From Fig. 5 it can be seen that the oxygen is only present on the surface, while nitrogen has diffused into interior.

Over a year in Sichuan environment (ambient temperature, 70% relative humidity), the nitrided sample turned yellow but still had metallic luster. The non-nitrided sample became progressively darker, lost its reflective properties, non-adherent oxide layer formed. In Fig. 6 the XRD spectra of non-nitrided sample and nitrided sample are presented. It can be seen that UO_2 formed on the non-nitrided sample. As the major peaks for U_2N_3 and UO_2 overlap, only the increased intensity of peak at $\theta = 28.5^\circ$ can be attributed to UO_2. In order to show how the amount of UO_2 vary with time, a simple method is adopted. The fractional intensity of the peak at $\theta = 28.5^\circ$ attributed to UO_2 is calculated by using area of peak at $\theta = 28.5^\circ$ divided area of all peaks from $\theta = 25^\circ$ to $\theta = 45^\circ$. Fig. 6 presents the fractional intensity of peak at $\theta = 28.5^\circ$ vary with time, the UO_2 of non-nitrided uranium grows steadily, however the UO_2 of nitrided sample ceased to grow after 2 months. XPS depth profile of nitrided sample kept 1 year in the ambient environment (Fig. 5) shows the thickness of the oxide layer is not more than 10 nm. Under hot–humid test (temperature 90 °C, humidity 95%), the corrosion rate of the nitrided sample is strongly reduced comparing to non-nitrided uranium as revealed by XRD (Fig. 7). After 12 h, the non-nitrided sample corroded heavily, the shiny surface turned black and a loose oxide layer forms that can easily flake off. After 20 days the laser nitrided sample turned blue, the oxide film is still protective as shown in Fig. 8. XPS depth profile reveals that oxygen diffuse deeply into nitrided layer, The outmost oxygen forms UO_2, its thickness is not more than 80 nm (Fig. 5). The depth profile of nitrogen shows that as corrosion proceeds nitrogen tends to diffuse deeper in the specimen, the same trend is observed as for the long-term amorphisation of C and N implanted layers on a uranium surface reported by Arkush et al. [12]. However, as compared to Arkush et al.'s experiments, the amorphisation of the laser nitrided layer is less than for the ion implantation layer. An additional experiment examining the thermostability of the nitride layer was performed by annealing sample at 300 °C for 24 h in high vacuum chamber, which shows no sign of amorphisation. The reason may lies in the fact that the UN is more stable than UN_2 and U_2N_3.

4. Conclusion

A nitride layer is formed by excimer laser irradiation, which is composed of mainly UN and U_2N_3 and depends on nitriding process. The amount of nitride increase with energy density and pressure. The irradiated area has a wavy structure which increases the roughness, while scratches and asperities caused by sand paper were eliminated. Scan speed has profound influence on the nitride layer, at low speed U_2N_3 is more likely to form and the nitride layer tends to crack. XPS analysis shows that nitrogen diffuses into interior, while oxygen is only present on the surface. Ambient and hot–humid corrosion tests show that the nitrided material has good anticorrosion property.

Acknowledgements

The authors would like to acknowledge Lizhu Luo, Shiyong Tan for XPS analysis and Chunli Jiang Huogen Huang, Tingting Liu for the XRD and SEM analysis. This work was supported by the Science and Technology Foundation of China Academy of Engineering Physics under contract number 2007B07001.

References

[1] D.M. Mattox, R.D. Bland, J. Nucl. Mater. 21 (1967) 349–352.
[2] C.M. Egert, D.G. Scott, J. Vac. Sci. Technol. A 5 (1987) 2724–2727.
[3] E.N. Kaufmann, R.G. Musket, C.A. Colmenares, B.R. Appleton, CONF-831174-80.
[4] R. Arkush, M.H. Mintz, N. Shamir, J. Nucl. Mater. 281 (2000) 182–190.
[5] C. Boulmer-Leborgne, A.L. Thomann, J. Hermann, SPIE 2207 (1994) 513–524.
[6] A.L. Thomann, E. Sicard, C. Boulmer-Leborgne, C. Vivien, J. Hermann, C. Andreazza-Vignolle, P. Andreazza, C. Meneau, Surf. Coat. Technol. 97 (1997) 448–452.
[7] T.M. Yue, J.K. Yu, H.C. Man, Surf. Coating. Technol. 137 (2001) 65–71.
[8] P. Schaaf, Prog. Mater. Sci. 47 (2002) 1–161.
[9] G.C. Allen, P.M. Tucker, J.W. Tyler, J. Phys. Chem. 86 (1982) 224–228.
[10] S.V. Chong, H. Idriss, Surf. Sci. 504 (2002) 145–158.
[11] P.R. Norton, R.L. Tapping, D.K. Creber, W.J.L. Buyers, Phys. Rev. B 21 (1980) 2572–2577.
[12] R. Arkush, M.H. Mintz, G. Kimmel, N. Shamir, J. Alloys Compd. 340 (2002) 122–126.
[13] Ingmar Grenthe, Janusz Drożdżyński, Takeo Fujino, et al., in: Lester R. Morss, Norman M. Edelstein, Jean Fuger, Joseph J. Katz, The Chemistry of the Actinide and Transactinide Elements, Springer, 2006, p. 407.